Bioactive Materials 21 (2023) 209–222

Contents lists available at ScienceDirect

Bioactive Materials

journal homepage: www.keaipublishing.com/en/journals/bioactive-materials

Assessing the response of human primary macrophages to defined fibrous architectures fabricated by melt electrowriting

Carlotta Mondadori [a,1], Amit Chandrakar [b,1], Silvia Lopa [a,1], Paul Wieringa [b], Giuseppe Talò [a], Silvia Perego [c], Giovanni Lombardi [c,d], Alessandra Colombini [e], Matteo Moretti [a,f,g,h,*], Lorenzo Moroni [b,**]

[a] IRCCS Istituto Ortopedico Galeazzi, Cell and Tissue Engineering Laboratory, Milan, Italy
[b] Complex Tissue Regeneration Department, MERLN Institute for Technology-Inspired Regenerative Medicine, Maastricht, the Netherlands
[c] IRCCS Istituto Ortopedico Galeazzi, Laboratory of Experimental Biochemistry and Molecular Biology, Milan, Italy
[d] Department of Athletics, Strength and Conditioning, Poznań University of Physical Education, Poznań, Poland
[e] IRCCS Istituto Ortopedico Galeazzi, Orthopaedic Biotechnology Lab, Milan, Italy
[f] Regenerative Medicine Technologies Lab, Ente Ospedaliero Cantonale, Bellinzona, Switzerland
[g] Service of Orthopaedics and Traumatology, Department of Surgery, Ente Ospedaliero Cantonale, Lugano, Switzerland
[h] Euler Institute, Faculty of Biomedical Sciences, Università della Svizzera Italiana, Lugano, Switzerland

ARTICLE INFO

Keywords:
Macrophage
Melt electrowriting
Additive manufacturing
Scaffold design
Scaffold geometry

ABSTRACT

The dual role of macrophages in the healing process depends on macrophage ability to polarize into phenotypes that can propagate inflammation or exert anti-inflammatory and tissue-remodeling functions. Controlling scaffold geometry has been proposed as a strategy to influence macrophage behavior and favor the positive host response to implants. Here, we fabricated Polycaprolactone (PCL) scaffolds by Melt Electrowriting (MEW) to investigate the ability of scaffold architecture to modulate macrophage polarization.

Primary human macrophages unpolarized (M0) or polarized into M1, M2a, and M2c phenotypes were cultured on PCL films and MEW scaffolds with pore geometries (square, triangle, and rhombus grid) characterized by different angles.

M0, M2a, and M2c macrophages wrapped along the fibers, while M1 macrophages formed clusters with rounded cells. Cell bridges were formed only for angles up to 90°. No relevant differences were found among PCL films and 3D scaffolds in terms of surface markers. CD206 and CD163 were highly expressed by M2a and M2c macrophages, with M2a macrophages presenting also high levels of CD86. M1 macrophages expressed moderate levels of all markers. The rhombus architecture promoted an increased release by M2a macrophages of IL10, IL13, and sCD163 compared to PCL films. The proangiogenic factor IL18 was also upregulated by the rhombus configuration in M0 and M2a macrophages compared to PCL films.

The interesting findings obtained for the rhombus architecture represent a starting point for the design of scaffolds able to modulate macrophage phenotype, prompting investigations addressed to verify their ability to facilitate the healing process in vivo.

1. Introduction

Macrophages are cells of the innate immune system that protect the body from pathogenic infections [1]. Beyond their main immunological function, macrophages are crucially involved in other mechanisms, such as the maintenance of body homeostasis and tissue repair in response to damages. Despite their positive contribution to tissue repair in the first phases of tissue healing, macrophages can also significantly contribute to the pathogenesis and progression of various inflammatory diseases when they abnormally infiltrate and accumulate in tissues [2,3]. Based

Peer review under responsibility of KeAi Communications Co., Ltd.
* Corresponding author. IRCCS Istituto Ortopedico Galeazzi, Cell and Tissue Engineering Laboratory, Milan, Italy.
** Corresponding author.
E-mail addresses: matteo.moretti@grupposandonato.it (M. Moretti), l.moroni@maastrichtuniversity.nl (L. Moroni).
[1] Carlotta Mondadori, Amit Chandrakar, and Silvia Lopa contributed equally to this work.

https://doi.org/10.1016/j.bioactmat.2022.07.014
Received 29 December 2021; Received in revised form 30 June 2022; Accepted 11 July 2022

on a simplified classification that describes the different polarization state of macrophages, they can be designated as classically (M1) and alternatively (M2) activated macrophages. M1 and M2 macrophages are respectively considered as pro- and anti-inflammatory cells, which represent the two extremes of a continuous macrophage phenotype spectrum [4]. When unpolarized macrophages (M0) polarize towards an M1 phenotype, they express high levels of pro-inflammatory mediators, such as TNF-α and IL-1β, driving and amplifying the inflammatory response. On the other hand, M2 macrophages exert anti-inflammatory effects by releasing anti-inflammatory mediators, such as IL-10 and IL-1Ra, thus facilitating tissue repair and remodeling [5]. M2 macrophages can be further divided into different subtypes, M2a, M2b, and M2c with slightly different roles: M2a and M2b exert immunomodulatory functions, while the M2c subset is more related to tissue remodeling and to the suppression of immune responses [6]. This heterogeneity of functions allows macrophages to play multiple roles in inflammation and tissue repair, promoting or counteracting these processes depending on their phenotype. Unlike other terminally differentiated cells, macrophages are unique due to the intrinsic plasticity that allows them to switch between distinct functional phenotypes in response to microenvironmental signals [7]. Indeed, the polarization state is transient and M1 macrophages can be reprogrammed to M2 following exposure to wound healing stimuli, whereas M2 macrophages can switch to M1 when stimulated by inflammatory signals [8]. Based on this specific feature, modulating macrophage phenotype has been proposed as an innovative approach to turn an inflamed milieu into a healing-friendly environment and modulate the inflammatory state [9–11]. In fact, while the inflammatory M1 response is crucial to initiate the healing process, the prolonged presence of M1 macrophages is detrimental and leads to chronic inflammation. In this context, favoring the polarization of macrophages into phenotypes exerting anti-inflammatory functions and promoting tissue remodeling and regeneration is a promising approach to improve the performances of implanted biomaterials.

The current understanding on macrophage polarization and plasticity is mostly limited to how soluble biochemical factors, including cytokines, influence macrophage polarization [12,13]. However, multiple evidences support the idea that macrophage phenotype can also change in response to biophysical cues [14–16]. In particular, an interesting insight has been provided by the idea of being able to influence macrophage polarization acting on cell shape and exploiting molecular pathways that transduce physical cues and modulate cell behavior [16]. Therefore, one of the possible strategies to induce macrophage skewing is to exploit rationally-designed biomaterials [17]. Based on this premise, the elucidation of how the 3D structure and geometry of a material can affect macrophage response has recently gained rising interest [17–19]. This represents a new opportunity for rational scaffold design which, until now, has primarily focused on tuning the geometric features of biomaterial scaffolds, for instance in terms of pore size and shape, as drivers of tissue regeneration. Instead, the exploitation of these same features to create a healing-friendly environment by acting on immune cells involved in foreign body reaction provides a promising alternative to biomaterial applications.

To generate 3D scaffolds with specific geometric features, different manufacturing techniques have been exploited. The majority of the available studies have used electrospinning, since this fabrication technique allows obtaining fibers and pore size in the range of the cell dimensions [20]. These studies have been mostly focused on the role of pore size alone [21] or combined with fiber size [22,23] on macrophage polarization. However, in the process of electrospinning, fiber and pore dimensions increase linearly and, therefore, are intrinsically linked to each other [24]. As a consequence, it is not possible to produce scaffolds with small fibers and large pores or vice versa, making this technique poorly controllable. Electrospinning allows the fabrication of scaffolds with random or aligned fibers [25], but it is not compatible with the production of scaffolds with precisely oriented fibers and specific geometric patterns. As an alternative to electrospinning, additive manufacturing has been exploited to investigate the impact of scaffold architecture on cell behavior, demonstrating that fiber orientation and pore geometry affect cytokine production by human monocytes [26]. Although additive manufacturing techniques allow a precise control over scaffold architecture, the fiber size of the fabricated scaffolds is often out of the cell dimension range. Indeed, cells tend to behave similarly to those cultured in 2D conditions since fibers are too large for them to recognize the scaffold as a 3D environment [27].

In this scenario, Melt Electrowriting (MEW) is a recently developed technology that bridges the gap between solution-based electrospinning and other conventional additive manufacturing techniques [28]. MEW allows the fabrication of scaffolds with fibers of few microns, comparable to the extracellular matrix of many tissues, while precisely controlling fiber deposition. These features permit to obtain precise scaffold architectures with tunable geometric parameters, such as fiber orientation, fiber size, pore geometry, and pore size [29]. Moreover, differently from electrospinning, MEW can generate scaffolds with different fiber size while keeping constant the pore size and vice versa, which permits to analyze separately the contribution of different parameters to cell behavior. For all these reasons, MEW can be exploited to identify geometrical cues affecting macrophage behavior. Although MEW is an emergent technique, it has already yielded interesting insights in the influence of 3D scaffold architecture on cell behavior [30,31], beyond the several biomedical applications it is useful for [32]. In particular, the recent paper from Tylek et al., which was published while the present study was already ongoing, has highlighted how the size of box shaped pores in PCL scaffolds obtained by MEW affects macrophage phenotype, most likely due to cell elongation across multiple pores in the case of small pores (i.e. 40 μm).

Herein, the behavior of pre-differentiated macrophages, either unpolarized (M0) or polarized towards different phenotypes, was investigated in response to pore geometries characterized by different angles between adjacent fibers. This approach was specifically chosen to investigate the ability of different architectures to induce the polarization toward a specific phenotype in the case of unpolarized macrophages and the ability to induce phenotype switching in the case of polarized macrophages. To this aim, we generated 3 different pore geometries (square, triangle, and rhombus) by orienting the fibers in such a way that different angles could be formed. The selection of this strategy was based on the idea to investigate the influence of the geometry of intersecting fibers on cell behavior. Specifically, our aim was to test conditions facilitating the stretching of cells across crossing fibers and inducing the formation of cell bridges or conditions hampering this event. Since we wanted to investigate the response of primary human macrophages, monocytes were isolated from peripheral blood and differentiated for 5 days to obtain macrophages. Macrophages were subsequently maintained for 2 further days in M0 conditions or polarized into M1, M2a or M2c phenotypes using polarizing cytokines, before being seeded on MEW scaffolds. After 3 days of culture, we investigated the response of the different macrophage phenotypes to geometric features, assessing how the scaffold architecture affected cell morphology, surface marker expression, and cytokine/chemokine secretion.

2. Materials and methods

2.1. Materials, 3D scaffold fabrication and characterization

A commercially available MEW system from SprayBase (Fig. 1a) was used to fabricate the scaffolds. As shown in Fig. 1b, this is a pressure driven system that controls and allows the extrusion of a given polymer through the nozzle. Three different scaffold architectures were fabricated considering different polygons as the elementary unit of the entire scaffold: i) square grid ii) equilateral triangle grid, and iii) rhombus grid. Specifically, fibers were deposited to obtained different types of angles between fibers of adjacent layers. In the case of square and equilateral triangle grids all the angles were respectively of 90° and 60°, while in

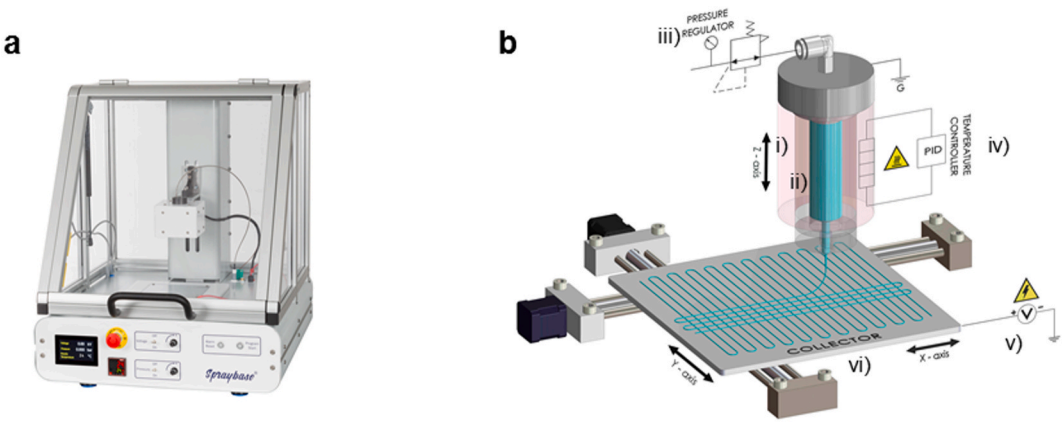

Fig. 1. MEW system to generate 3D scaffolds with highly controlled architecture. (a) SprayBase machine used to generate different scaffold architectures. (b) Basic schematic of any pressure driven melt electrowriting system. The system consists of: i) a syringe where polymer melts are housed, ii) a heater element to melt the polymer pellets, iii) a pressure regulator that controls the pressure and the extrusion of the polymer from the nozzle, iv) a proportional–integral–derivative (PID) temperature controller to accomplish the heating to melt the polymer, v) a high voltage supply connected either to a collector or to a syringe or in some cases to both of them and vi) a moving collector to draw a straight fiber.

the case of rhombus grid two angles were of 150° and two of 30°. The manufacturing parameters for the square, triangle, and rhombus grid scaffolds are listed in Table 1.

For scaffold fabrication, pellets of polycaprolactone (PCL, average Mn 45,000, Sigma-Aldrich) were loaded into a syringe (internal diameter: 16 mm, external diameter: 30 mm) and heated up to 80 °C for 20 min before extrusion. A positive voltage was applied to the nozzle, while the steel collector plate was grounded. The distance between the nozzle and the collector plate was set at 4 mm. PCL was extruded through the needle using 0.4 bar air pressure. After the polymer jet was stabilized, fibers were directly written onto the collector plate that moved with different speed based on the different scaffold geometries. The syringe was cleaned and loaded with new material every 9 h to avoid any material degradation. Morphological analysis of the different scaffold architectures was carried out by scanning electron microscopy (SEM; FEI Teneo, Philips). ImageJ was used to measure fiber diameter, and pore size. The straight-line and the angle selection tool of ImageJ software were used to measure fiber diameters and angles formed between fibers, respectively. Three different scaffolds were analyzed for each architecture, with 8 random measurements taken from each scaffold (24 measurements per architecture) to calculate the mean fiber diameters and fiber angles.

2.2. 2D film fabrication

PCL films were used as 2D control group and were obtained by a hot-embossed compression molding technique. Briefly, PCL pellets were distributed inside circular molds (Ø 10 mm) of a stainless steel that was placed between two silicon wafers functionalized with 1H,1H,2H,2H-perfluorodecyltrichlorosilane (FDTS, Sigma-Aldrich). The wafer-mold-wafer sandwich was placed in the hot press (Atlas Series Heated Platens, Specac) setting the temperature and the pressure at 80 °C and 5 bar, respectively. After 5 min, the system was cooled to 30 °C, the pressure was released and the mold was separated from the wafers by soaking them in pure ethanol for 5 min to facilitate their separation. The smooth films were obtained by detachment from the circular molds.

Table 1
Manufacturing parameters for the fabrication of square, triangle, and rhombus MEW scaffolds.

Scaffold geometry	Melt temperature (°C)	Air pressure (bar)	Nozzle voltage (kV)	Collector distance (mm)	Collector speed (mm/s)
Square	80	0.4	5	4	80
Triangle	80	0.4	5.25	4	70
Rhombus	80	0.4	5	4	80

2.3. Monocyte isolation, macrophage differentiation and polarization

Human primary monocytes were isolated by Ficoll (GE Healthcare) density gradient separation and $CD14^+$ selection using CD14 microbeads (MACS, Miltenyi) [33] from buffy coats of healthy donors purchased from the local blood bank. After isolation, $CD14^+$ monocytes were cultured in complete medium made of RPMI-1640 (Gibco) supplemented with 20% heat-inactivated FBS (Hyclone) and 1% penicillin-streptomycin-glutamine (PSG, Thermofisher Scientific) at a density of 0.3×10^6 cells/cm^2 for 5 days in T25 flasks. Macrophage colony-stimulating factor (M-CSF, Peprotech) was added to culture medium at 20 ng/mL to differentiate monocytes into macrophages. After 5 days, macrophages were polarized to specific phenotypes by exposing them to different cytokines (all from Peprotech) for 2 days as follows [34]: 100 ng/mL IFNγ and 100 ng/mL TNFα were used to obtain M1 macrophages, 40 ng/mL IL4 and 20 ng/mL IL13 to obtain M2a macrophages and 40 ng/mL IL10 to obtain M2c macrophages. All polarizing media contained M-CSF at 20 ng/mL. Unpolarized macrophages (M0) were cultured without polarizing cytokines, but only with 20 ng/mL M-CSF. Each experiment was repeated with cells obtained from at least 3 different blood donors.

2.4. Characterization of macrophage phenotypes by flow cytometry

To analyze macrophage immunophenotype, primary human monocytes were differentiated for 5 days in the presence of 20 ng/mL M-CSF and then maintained unpolarized (M0) or polarized towards M1, M2a, and M2c phenotypes for 2 days. At this timepoint (d0), corresponding to the timepoint of macrophage seeding on tissue culture plates (TCP), PCL films and scaffolds, some macrophage plates were detached and analyzed by flow cytometry to assess the expression of typical macrophage phenotypic markers (CD86, CD206, CD163). Other plates were cultured for 3 additional days without adding any cytokine to mimic the timeframe and the experimental conditions used for macrophage experiments on TCP, PCL films and scaffolds, before performing flow cytometry.

For cell harvesting, macrophages were washed with PBS, detached by incubation with non-enzymatic cell dissociation buffer (Thermofisher Scientific) for 7 min and centrifuged at 500g for 5 min. Afterwards, 10^5 macrophages were suspended in 100 μL MACS buffer (Miltenyi Biotec) and stained to evaluate the expression of surface markers with the

following antibodies, after being pre-incubated with FcR blocking reagent (Miltenyi Biotec): anti-human CD86-FITC (Clone REA968, 1:50, Miltenyi Biotec), anti-human CD206-PE (Clone DCN228, 1:50, Miltenyi Biotec), and anti-human CD163-PE-Vio770 (REA812, 1:50, Miltenyi Biotec). Unstained cells were used as negative control for fluorescence. All the stains were performed at 4 °C for 20 min in the dark. Data were acquired using a Cytoflex flow cytometer (Beckman Coulter Inc.).

2.5. Cell seeding

MEW scaffolds were punched to a diameter of 14 mm and placed in non-treated 24-well plates (Greiner BioOne) where they were sterilized with 70% ethanol for 30 min followed by evaporation for 2 h. After ethanol evaporation, sterile Viton O-rings (internal Ø 11.89 mm, cross section 1.98 mm, Eriks) were placed in each well to prevent the scaffolds from floating. PCL films were punched to a diameter of 10 mm, sterilized with 70% ethanol and placed in non-treated 48-well plates using sterile Viton O-rings (internal Ø 9.5 mm, cross section 1 mm, Eriks). The lower diameter of PCL films compared to PCL scaffolds was necessarily selected to reduce the probability of film wrapping during sample handling. Afterwards, scaffolds and films were incubated overnight in complete medium to provide protein attachment before cell seeding.

After 7 days of culture (5 days of differentiation and 2 days of polarization), M0, M1, M2a and M2c macrophages were detached as above described and counted. Similar to 3D scaffolds, TCP samples were seeded in 24 well plates, while PCL films were seeded in 48-well plates. For all the conditions, a seeding density of 0.1×10^6 cells/cm^2 was applied (corresponding to a total amount of 0.2×10^6 cells for TCP and 3D scaffolds in 24-well plates and 0.1×10^6 cells for PCL films in 48-well plates). For PCL scaffolds, to avoid the interference of cells deposited through the pores on the bottom surface of the wells, PCL scaffolds were transferred to clean wells 3 h after cell seeding. Cells were cultivated for 3 days on scaffolds or films, in line with previous studies testing macrophage response to biomaterials [22,35,36]. In this last phase, culture medium (RPMI-1640 with 10% heat-inactivated FBS and 1% PSG) did not contain M-CSF or polarizing cytokines.

2.6. Scanning electron microscopy (SEM)

For SEM analysis, macrophages were cultured on 3D scaffolds and PCL films were used as 2D control. After 3 days, samples were fixed using 2% formaldehyde methanol-free (Thermofisher Scientific) for 15 min. After that, samples underwent dehydration by a graded ethanol series (30%, 50%, 70%, 80%, 90%, 96% and 100% ethanol, 15 min for each step). Dehydrated samples were incubated with ethanol:hexamethyldisilazane (HMDS, Sigma-Aldrich) series (75:25, 50:50, 25:75, 0:100, 15 min for each step). After HMDS was evaporated, samples were placed on stubs and sputter-coated with a conductive gold layer (108 auto, Cressington Scientific Instruments) prior to SEM imaging. To determine cell morphology on PCL films and scaffolds, SEM images were taken at a magnification of 2500X. Specifically, for cells seeded on MEW fabricated scaffolds, the images were taken at fiber intersections to evaluate the morphology of cells close to different angles.

2.7. F-actin and immunofluorescence staining of cell surface markers

For F-actin staining and surface marker analysis by immunofluorescence, cells were cultured on top of 3D scaffolds and PCL films were used as 2D control groups. Samples were fixed using 2% formaldehyde methanol-free for 15 min. For F-actin staining, cell membranes were permeabilized with 0.1% Triton X-100 in PBS for 10 min, washed in PBS and incubated with Phalloidin-iFluor 488 (A12379, 1:70, Thermofisher Scientific) in 1% bovine serum albumin (BSA, Sigma-Aldrich) for 1 h at RT, before nuclear staining. For immunofluorescence staining of cell surface proteins, cells were incubated with 2% BSA and FcR blocking reagent (blocking medium) for 30 min at RT, and subsequently incubated at 4 °C overnight with primary antibodies. Specifically, a double immunostaining was performed to detect CD86 using a mouse monoclonal antibody (sc-19617, 1:100, SantaCruz Biotechnology), together with CD206 or CD163 using rabbit polyclonal antibodies (ab64693, 1:500, Abcam; ab87099, 1:200, Abcam) [6]. After washing in PBS, samples were incubated 1 h at RT with secondary antibodies: goat anti-mouse AlexaFluor-647 (A21235, 1:1000, Thermofisher Scientific) and goat anti-rabbit AlexaFluor-488 (A11008, 1:500, Thermofisher Scientific). For both F-actin and immunofluorescence staining, nuclei were stained with 600 nM 4′,6-diamidino-2-phenylindole (DAPI, Sigma-Aldrich) for 30 min at RT. Samples were mounted on slides with the antifade mounting medium (Thermofisher Scientific) and observed by confocal microscopy. Leica SP5 with 40X objective was used for imaging F-actin, whereas Leica SP8 with 10X objective was used for imaging cell surface markers.

2.8. Cytokine/chemokine quantification via multiplex immunofluorescence assay

For cytokine quantification via multiplex assay, unpolarized and polarized macrophages from 3 independent blood donors were cultured on top of MEW scaffolds, on PCL films, and in 24-well TCP, with the last two groups representing the control groups. In each independent experiment, for each experimental condition, the supernatants for cytokine/chemokine analysis were pooled from 2 or 3 sample replicates. The number of replicates depended on the available number of macrophages for each blood donor. For the analysis, supernatants were collected at day 3 after cell seeding, centrifuged at 476 g at 4 °C for 10 min, and stored at −80 °C for cytokine and chemokine quantification. The protein secretion profiles of macrophages were determined through a multiplex bead-based immunofluorescent assay (R&D Human Magnetic Luminex Customized Assay, R&D Systems Inc.) following the manufacturer's specifications. In brief, the supernatants were incubated for 2 h with a specific cocktail of antibodies pre-coated onto magnetic microparticles, followed by 1 h incubation with biotinylated antibodies cocktail and additional 10 min incubation with streptavidin-phycoerythrin conjugate (Streptavidin-PE), which binds to the biotinylated antibody. Finally, the microparticles were resuspended in buffer and read using a MagPix™ System (Bio-Rad Laboratories, Inc.). All samples were tested in duplicate. Data were analyzed by fitting a 5-parametric curve (Bio-PlexManager software, version 6.1.1, Biorad). The total amount of protein was normalized to the total DNA content per experimental group (pg protein/ng DNA). DNA was used as a surrogate of cell number to remove the possible bias of having a different amount of cells in the different culture conditions [31,37]. For each donor and protein, the values measured in M1, M2a, and M2c macrophages on TCP were expressed as fold increase with respect to the value measured in M0 macrophages on TCP that was set at 1. Likewise, for each donor and protein, the values measured in any macrophage phenotype cultured on PCL films or scaffolds were expressed as fold increase with respect to the value measured M0 macrophages on PCL films that was set at 1. For each protein, the values are visualized through a grey-to-red heatmap from the lowest value (light grey) to the highest value (dark red). A heatmap showing the values of pg protein/ng DNA through a grey-to-red scale and the dot plot graphs showing the fold increase data and the raw data obtained from 3 independent macrophage donors are provided as Supplementary Figures (SI1, SI2, SI3).

2.9. DNA quantification

DNA was measured with the CyQuant Cell Proliferation Assay kit (Thermofisher Scientific) to normalize protein secretion to the DNA content. To this aim, the samples from which we harvested the supernatants for the multiplex immunofluorescence assay (Luminex) were washed with PBS and stored at −80 °C. After 3 freeze-thawing cycles, each sample was added with 250 μL of proteinase K solution (1 mg/mL

in EDTA-Tris buffer, pH 7.6; Sigma-Aldrich) and incubated overnight at 56 °C. Afterwards, 250 μL of lysis buffer added with RNase (1:500, Thermofisher Scientific) was added to each sample and incubated at RT for 1 h. Subsequently, cell lysate was pooled from sample replicates, mixed with CyQuant GR dye 1:1, and incubated in the dark for 15 min. Fluorescence was measured at excitation and emission wavelengths of 480 and 520 nm, respectively, using a spectrophotometer (VICTOR X3 Multilabel Plate Reader, PerkinElmer Corporation). In this way, we quantified the total amount of DNA content of the replicates from which supernatants were harvested and pooled.

2.10. Statistical analysis

Each experiment was performed at least 3 times with independent primary donors. For flow cytometry data and protein secretion data (pg protein/ng DNA), after assessing data distribution, statistical analyses were conducted to determine significant differences among groups either within multiple macrophages phenotypes at the same time point (flow cytometry data) or within a single macrophage phenotype cultured in different conditions (protein secretion data) using a One-Way ANOVA for matched nonparametric data with a Dunn's multiple comparison test. Differences were considered as statistically significant for p-values below 0.05. All analyses were performed using GraphPad Prism (GraphPad Software).

3. Results

3.1. Characterization of MEW scaffolds

The highly controlled deposition of fibers, a specific characteristic of the MEW technique, allowed the fabrication of scaffold architectures composed by grids with different shapes: square, triangle and rhombus. SEM images showed that the selected instrument parameters allowed obtaining a consistent scaffold structure and precise angles, satisfying the design requirements (Fig. 2). Furthermore, SEM analysis showed the 3D structures of the scaffolds generated by layer-by-layer deposition. Two layers of fibers formed the 3D square and rhombus architectures, whereas the triangle architecture needed 3 fiber layers to be formed. Reproducibility of 3D structure fabrication was confirmed by 3 consecutive printing session for all the architectures. As reported in the table (Fig. 2), the mean value of the different angles was close to the expected value of 90°, 60°, and 150° for square, triangle and rhombus, respectively. The average fiber diameter was in the range of 17–20 μm.

3.2. Characterization of macrophage phenotypes

Differentiation from monocytes to macrophages during the 5 days of culture in medium supplemented with M-CSF was verified by daily evaluating changes in cell morphology and by assessing the positive expression of the pan-macrophage marker CD68 before starting the polarization phase (Supplementary Figure SI4). After macrophage polarization, the flow cytometry analysis included the assessment of the percentage of positive cells for each marker and the Mean Fluorescence Intensity (MFI) associated to the cell population for each marker (Fig. 3a

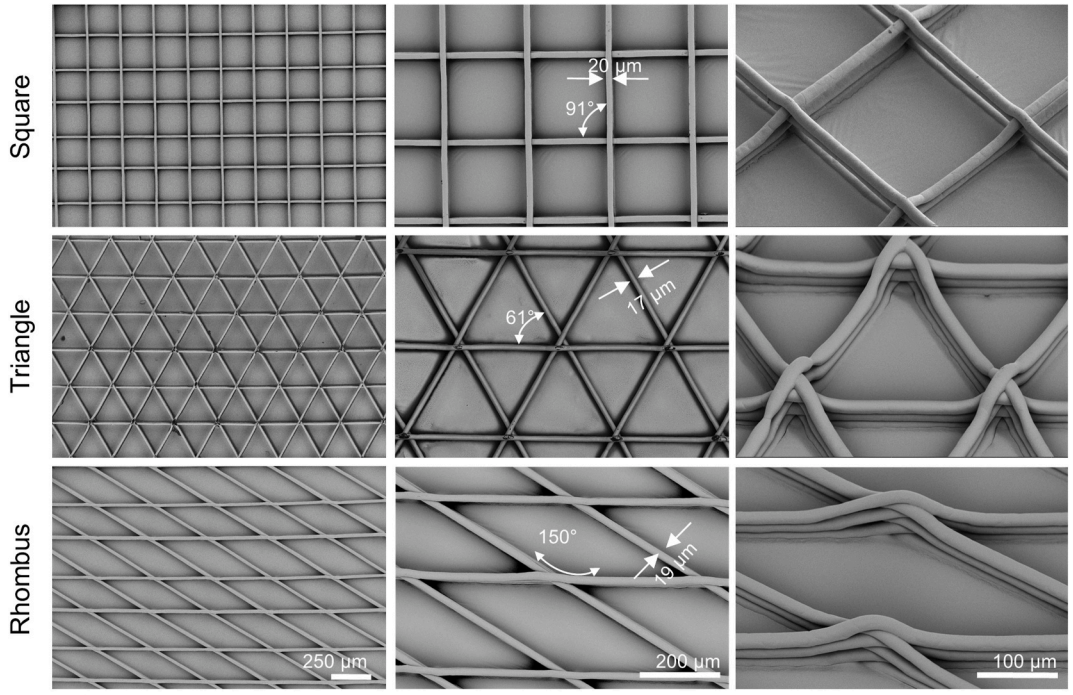

Scaffold geometry	Fiber size (μm)	Angle (°)
Square	20.49 ± 1.18	91.11 ± 1.21
Triangle	16.95 ± 1.15	61.00 ± 2.27
Rhombus	18.81 ± 1.75	149.98 ± 3.42

Fig. 2. SEM images of the 3 different geometric architectures with fiber and angle dimensions. Images in the first and second columns are top views, while images in the third column are perspective pictures showing the layer-by-layer fiber deposition. Fiber and angle size (mean ± standard deviation) is indicated in the table.

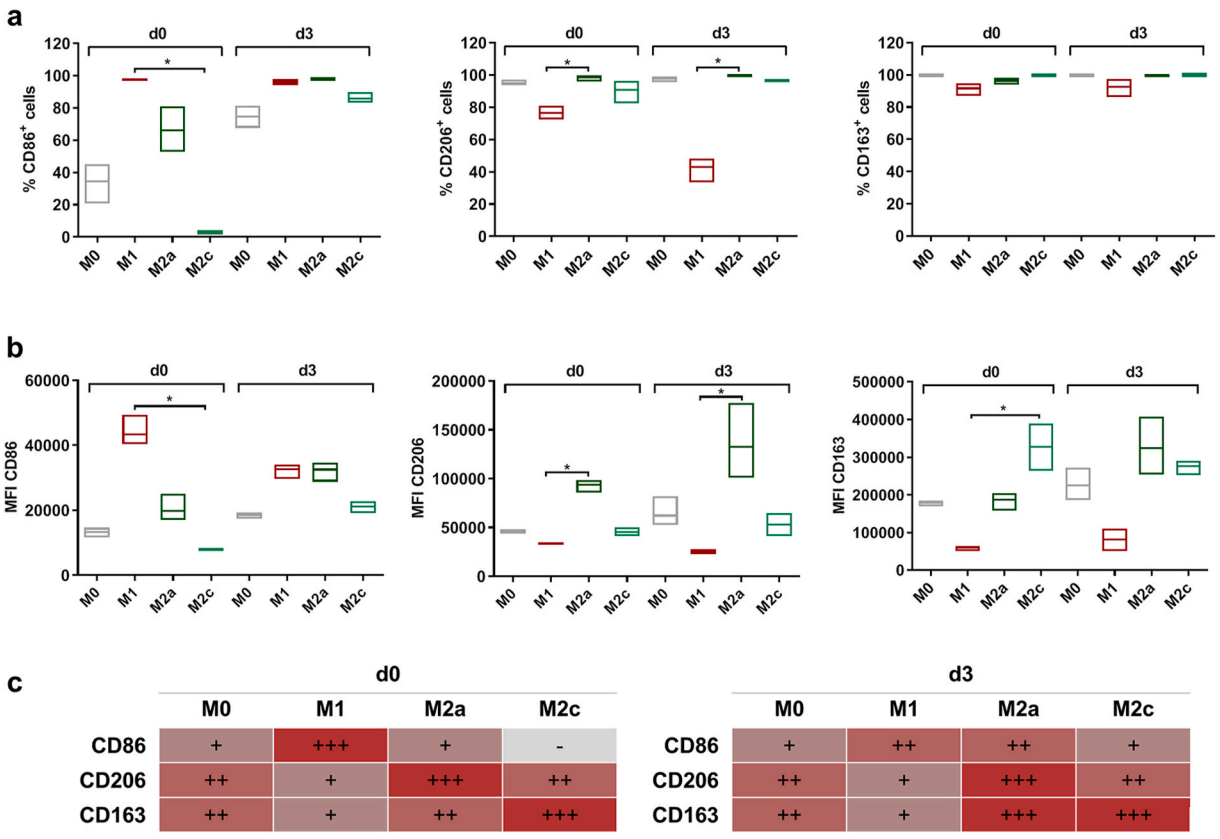

Fig. 3. Flow cytometric analysis of macrophage phenotype markers at the end of the polarization phase (d0) and after 3 additional days of culture without polarizing cytokines (d3). Floating bars show the percentage of cells positive for CD86, CD206, and CD163 (a) and the mean fluorescent intensity (MFI) per cell (b). Data are shown as min-to-max values with line at mean. The phenotypic profile of M0, M1, M2a, and M2c phenotypes at d0 and d3 is summarized in the table (c). Significant differences among single macrophage phenotype at the same time point are indicated (*$p < 0.05$).

and b). For what concerns the expression of CD86, at the end of the polarization phase (d0), this marker was clearly more expressed in M1 cells than in the other phenotypes, as shown both by the percentage of $CD86^+$ cells and by the MFI quantification. The lowest levels of this marker were measured in M2c macrophages, while M0 and M2a macrophages displayed an intermediate behavior. After 3 days of culture without polarizing cytokines (d3), the percentage of $CD86^+$ cells increased in M0, M2a, and M2c phenotypes, while the MFI decreased in M1 macrophages. These changes resulted in similar levels of CD86 in M1 and in M2a macrophages. Differently, the levels of CD86 remained lower in M0 and M2c macrophages. At both time points, the M2a marker CD206 was expressed at the lowest levels by M1 macrophages both in terms of percentage of $CD206^+$ cells and MFI. Differently, the M2c marker CD163 was expressed by the vast majority of cells in all the analyzed phenotypes, with a slightly inferior percentage of $CD163^+$ cells in M1 conditions. The analysis of the levels of this marker by MFI provided a clearer readout. In fact, at the end of the polarization phase (d0), M1 macrophages expressed the lowest levels of CD163, while the highest levels of this marker were detected in M2c macrophages, respectively. The low expression of M2 markers in M1 macrophages was maintained also after 3 days of culture without polarizing cytokines. Similarly, after 3 days without cytokines, M2a macrophages maintained very high levels of CD206 and displayed an increased expression of CD163, while M2c macrophages were characterized by the maintenance of high levels of CD163. These findings have been summarized providing a classification of the expression of these markers in the analyzed phenotypes at both time points (Fig. 3c).

3.3. Morphological analysis of macrophages cultured on MEW scaffolds

To observe the morphology of unpolarized (M0) and polarized macrophages (M1, M2a, M2c) cultured for 3 days on PCL films or scaffolds, we examined the actin cytoskeleton through Phalloidin staining (Fig. 4a and b). Macrophages assumed a different shape when seeded onto PCL films based on the different phenotype, with M0, M2a, and M2c macrophages showing a pancake morphology, and M1 macrophages characterized by a more elongated shape. These qualitative observations were corroborated by the quantitative analysis of cell morphology conducted through a customized ImageJ macro, which demonstrated that M1 macrophages were characterized by lower circularity and higher aspect ratio (ratio major axis/minor axis) compared to the other phenotypes (Supplementary Figure SI5). Conversely, when M1 macrophages were seeded on scaffolds they tended to form clusters of rounded cells with a more inhomogeneous distribution. On the other hand, M0, M2a, and M2c macrophages were mainly wrapped around the fibers, being more uniformly distributed than M1 macrophages. Moreover, M2a macrophages with multiple nuclei were observed on both PCL films and scaffolds suggesting that macrophage fusion occurred. Unfortunately, due to the impossibility to obtain a consistent cell segmentation starting from the Phalloidin staining of macrophages on MEW scaffolds, it was not possible to provide quantitative measures relative to the morphology of cells on PCL fibers.

Macrophage morphology was also observed by SEM (Fig. 5). Specifically, for cells seeded on top of scaffolds, images were taken at fiber intersection to precisely evaluate the morphology of cells close to different angles. SEM images confirmed the results obtained for the PCL films through actin staining. Indeed, M1 macrophages were

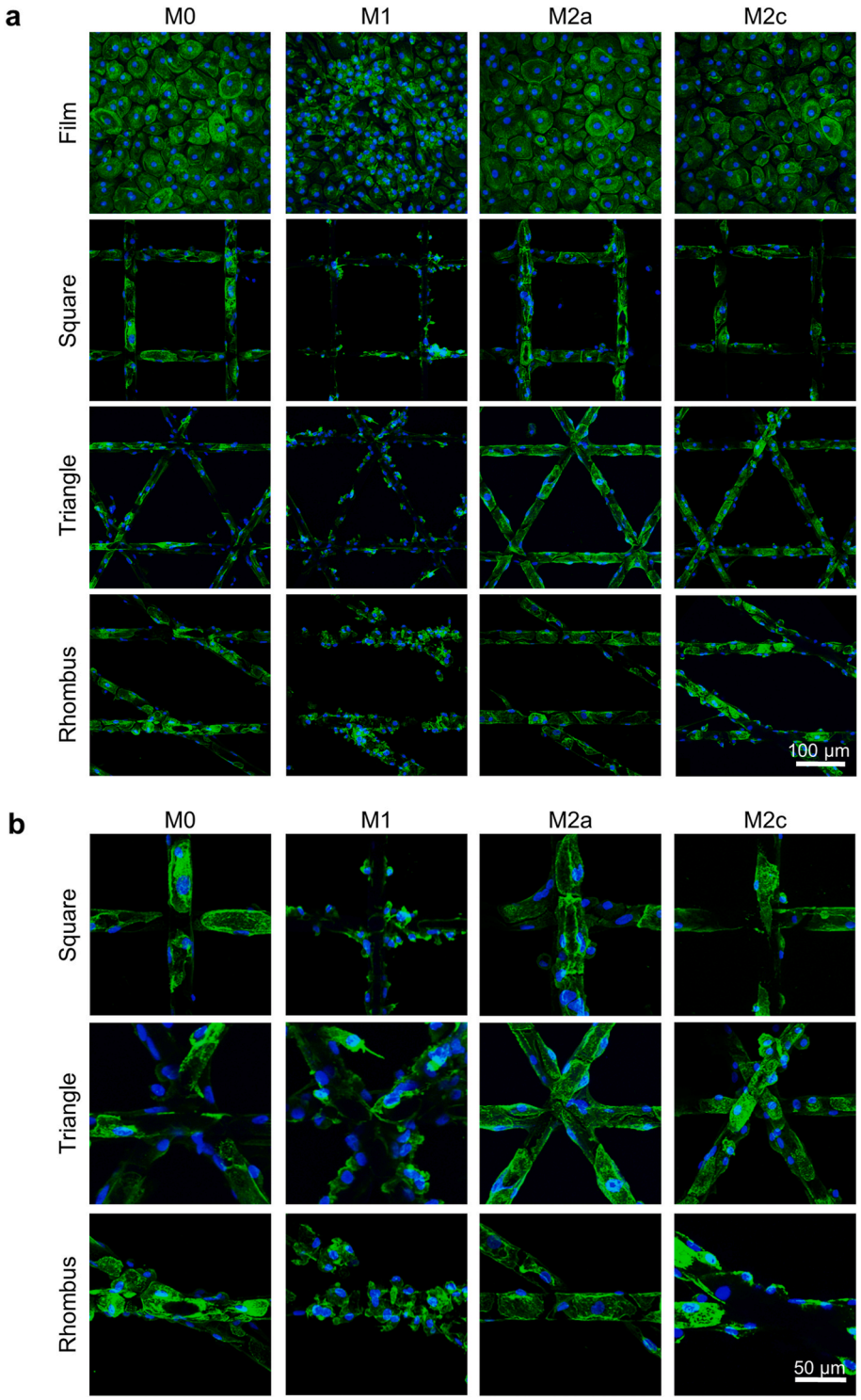

Fig. 4. DAPI and Phalloidin staining at lower (a) and higher (b) magnification to assess the morphology of unpolarized (M0) and polarized macrophages (M1, M2a, M2c) in contact with PCL films and scaffolds (square, triangle, and rhombus grid).

characterized by an elongated shape, whereas M0, M2a, and M2c macrophages had a more rounded shape. Moreover, SEM images of PCL films clearly showed the M2a macrophage fusion that was detected by actin staining. In correspondence of the 90° and 60° angles, macrophages elongated forming "cell bridges" between adjacent fibers on PCL scaffolds with square and triangle architecture. This behavior was evident in all the phenotypes for the triangle architecture, whereas it was observed only for M0 and M2 phenotypes in square scaffolds. Conversely, in the case of rhombus architecture, macrophages did not form any "cell bridge" in correspondence of the 150° angles. However, in correspondence of the 30° angle, cells showed the same behavior as for the square and triangle architectures (data not shown), with the elongation of cells between interconnecting fibers.

3.4. Expression of phenotype-associated cell surface markers

Immunofluorescence analysis was performed to evaluate the expression of surface markers, which are known to be differently

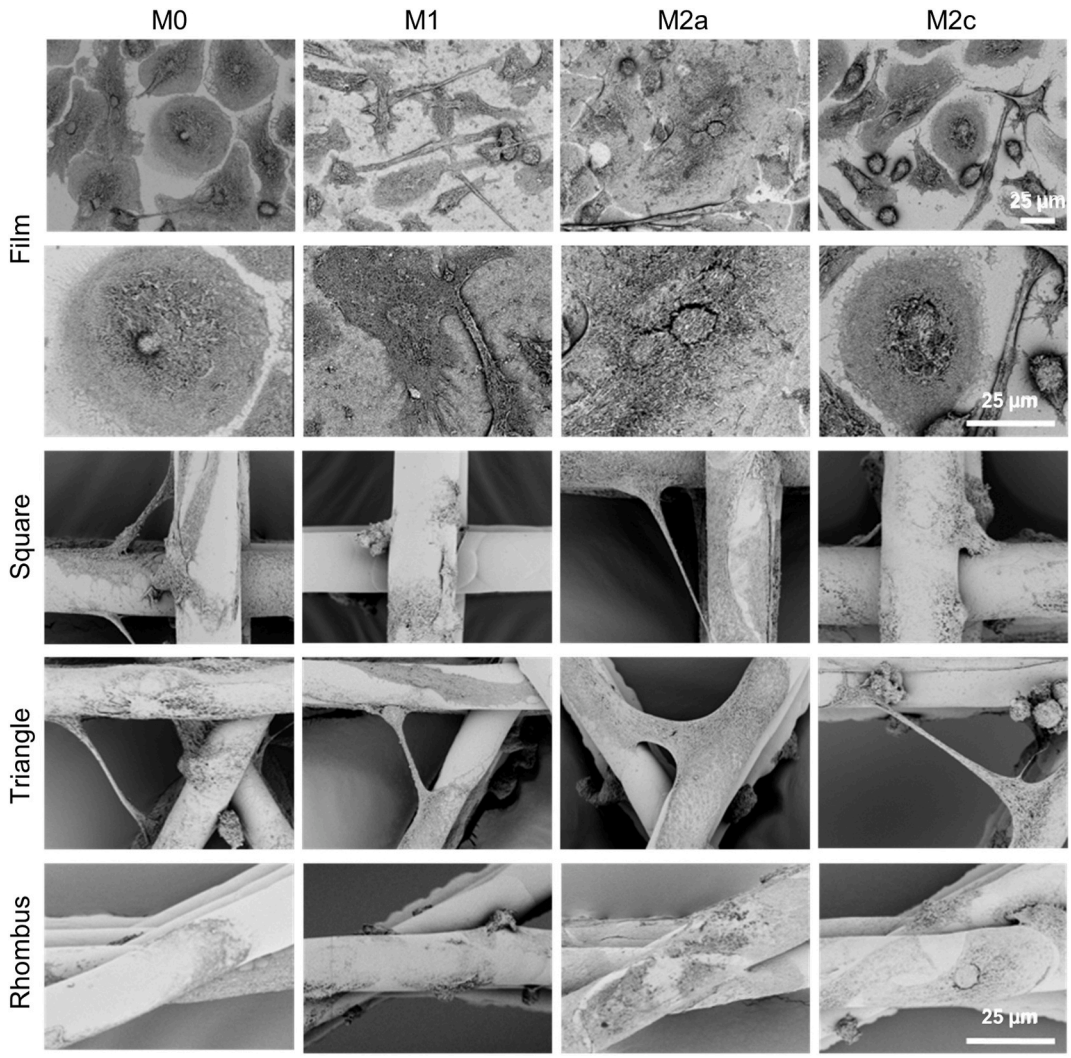

Fig. 5. SEM images showing the morphology of unpolarized macrophages (M0) and polarized macrophages (M1, M2a, M2c) in contact with PCL films and different scaffold architectures (square, triangle, and rhombus grid).

modulated in different macrophage phenotypes (Fig. 6a and b). As expected, the analysis of macrophages cultured on PCL films showed that CD206 and CD163 were expressed at the highest levels in M2a and M2c macrophages, respectively. The M2a phenotype was also characterized by a high expression of CD86, presenting a mixed population of cells highly positive for either CD206 only or for both CD206 and CD86. The lowest levels of CD86 were detected in M2c macrophages. M1 macrophages showed moderate levels of all the analyzed markers, differing from M2a and M2c macrophages mainly in terms of cell morphology, in line with the results provided by Phalloidin staining and SEM. These phenotypic features were maintained when macrophages were cultured on PCL scaffolds, with no clear change in terms of surface markers expression induced by any scaffold configuration.

3.5. Cytokine and chemokine secretion from macrophages on PCL films and scaffolds

To examine the ability of different geometric architectures in modulating the macrophage phenotype, we evaluated the secretion of cytokines and chemokines by unpolarized and polarized macrophages. Protein levels measured in different macrophage phenotypes cultured on TCP are presented as fold increase with respect to M0 macrophages on TCP to show macrophage behavior in standard 2D conditions (Fig. 7a). Protein levels secreted by macrophages cultured on PCL films and scaffolds are shown as fold increase with respect to the value measured in M0 macrophages on PCL films to emphasize the impact of scaffold architecture compared to cell-material interactions (Fig. 7b).

As expected, CCL5 and CXCL9, generally regarded as M1 markers, were strongly upregulated in M1 macrophages on TCP compared to M0 macrophages. In line with this data, the highest levels of CXCL9 were detected in M1 macrophages cultured on PCL films and scaffolds, with the triangle grid yielding the highest levels of CXCL9. No relevant differences in CXCL9 expression among 3D architectures were observed for M0, M2a, and M2c macrophages. The pro-inflammatory chemokine CCL5 was also strongly induced in M1 macrophages on TCP. Differently, the culture on PCL induced the expression of CCL5 specifically in M2a macrophages. Among the analyzed architectures, the rhombus grid was the one yielding the highest CCL5 expression in all phenotypes, except for M1 macrophages. The chemokine CCL7 that binds two of the main receptors involved in monocyte recruitment, CCR2 and CCR5, showed a trend similar to that of CCL5 for M0, M2a, and M2c phenotypes, while M1 macrophages in general expressed lower levels of CCL7 compared to M0 macrophages.

The analysis of chemokines typical of M2a activation showed that, among different macrophage phenotypes on TCP, CCL17 and CCL24 were expressed at similar levels. On the other hand, CCL22 was strongly induced in M2a macrophages on TCP compared to M0 macrophages. Considering M0 macrophages cultured on PCL films or scaffolds, the

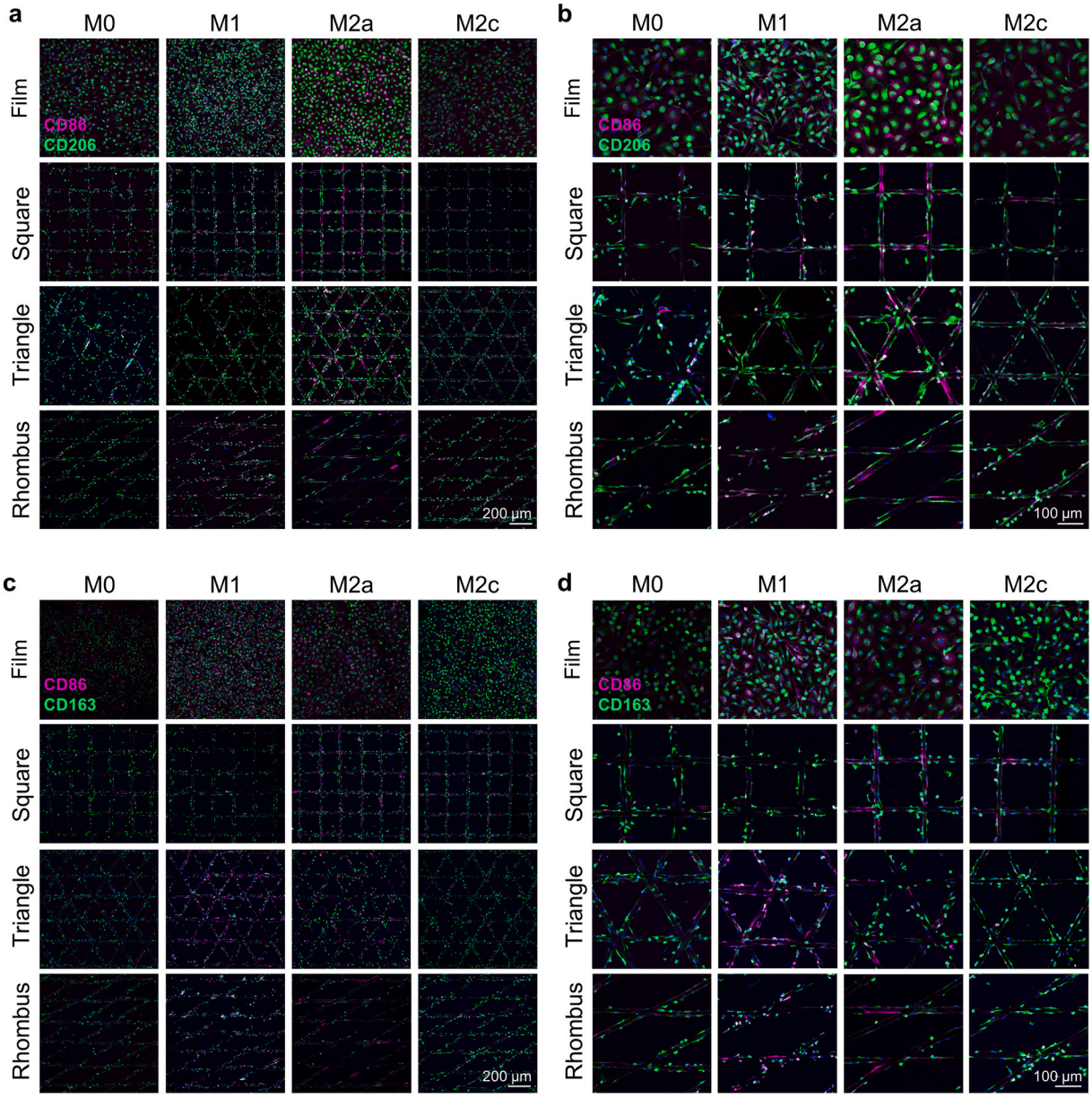

Fig. 6. Immunofluorescence staining of macrophage surface markers at different magnifications: (a,b) CD86 and CD206, (c,d) CD86 and CD163. In the pictures CD86 is shown in magenta, while CD206 and CD163 are shown in green.

highest levels of these markers were measured in cells cultured on the rhombus grid. Additionally, the rhombus grid yielded the highest levels of CCL17, CCL22, and CCL24 in M2a and M2c macrophages. For all macrophage phenotypes except M1, the pro-angiogenic chemokine CXCL2 was also strongly upregulated on the rhombus grid compared to the other scaffold architectures. The secretion of IL1β, TNFα, and IL6 was quite similar in all macrophage phenotypes, when cells were cultured on TCP, with the exception of the higher expression of IL6 in M2c macrophages. Except for the M1 condition, the levels of these markers were increased compared to PCL films when macrophages were cultured on any 3D scaffold architecture, with the highest increases found in M0 and M2a macrophages cultured on the rhombus architecture. Regarding anti-inflammatory interleukins, in the TCP condition the highest levels of IL1Ra were detected in M2a macrophages and the lowest in M1 macrophages, while the levels of IL10 remained stable among phenotypes. Among M0 macrophages on 3D scaffolds, the rhombus grid yielded the highest levels of IL1Ra and IL10. IL1Ra was strongly upregulated in M2a macrophages on PCL films and scaffolds, in line with the behavior observed on TCP films. Comparing the different architectures, the highest increase in IL1Ra was induced by the square grid, although this was mainly due to a single macrophage donor which strongly reacted to the square architecture. A more consistent increase in IL1Ra levels among different macrophage donors was induced by the rhombus architecture in all phenotypes except M1. Similarly to IL10 and IL1Ra, the anti-inflammatory cytokine IL13 was enhanced by the rhombus grid compared to the PCL film in any phenotype, except for the M1 phenotype where the levels of this cytokine remained low. Remarkably, the enhancement in IL10 and IL13 levels observed in M2a macrophages on the rhombus grid was statistically significant compared to M2a macrophages cultured on PCL films ($p < 0.05$). IL18 showed an expression trend very similar to IL13, with the rhombus grid yielding the highest levels of this cytokine in all phenotypes, except M1. In particular, the increases in IL18 levels were statistically significant in M0 and M2a macrophages on the rhombus grid, compared to the same macrophage phenotypes on PCL films ($p < 0.05$). The soluble form of CD163 (sCD163), a marker associated to the M2c phenotype, as confirmed by

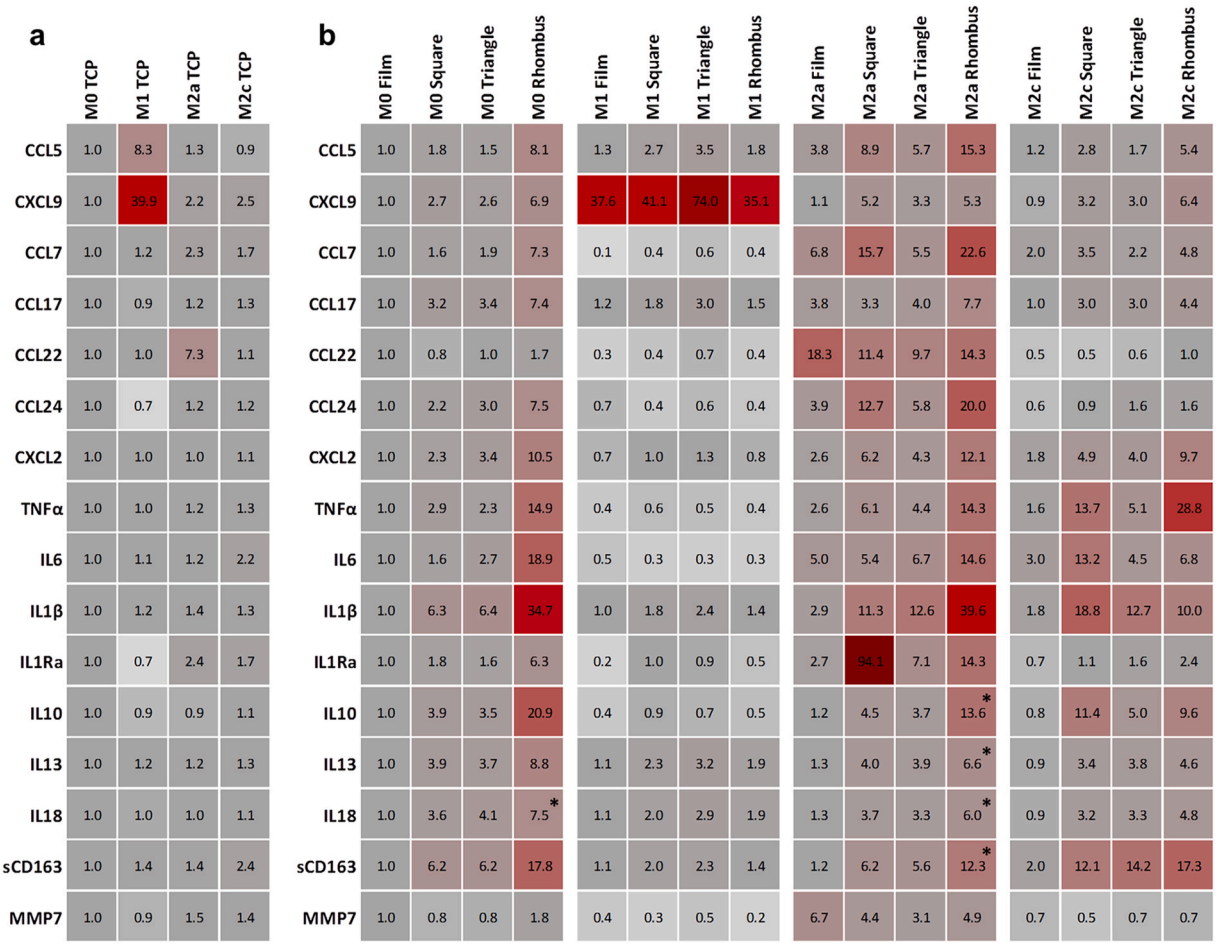

Fig. 7. Protein secretion analyzed via multiplex assay. (a) Protein secretion in TCP condition is represented as a grey-to-red heatmap showing the fold increase of each phenotype compared to M0 macrophages on TCP (set at 1). (b) Protein secretion by the different macrophage phenotypes (M0, M1, M2a, M2c) on PCL films or 3D scaffolds is represented as fold increase with respect to M0 macrophages on PCL films (set at 1) using a grey-to-red heatmap. The numbers in each square represent the average fold increase measured for 3 different macrophage donors. Significant differences within a single macrophage phenotype cultured on PCL films and 3D scaffolds are indicated in the square (Film vs. Rhombus $p < 0.05$).

macrophage behavior on TCP, was found to be expressed at the highest levels in M2c macrophages cultured on any scaffold configuration and on M0 and M2a macrophages on the rhombus grid. In particular, the levels of sCD163 were significantly higher in M2a macrophages cultured on this scaffold configuration than the same phenotype cultured on PCL films ($p < 0.05$). MMP7, a marker indicative of matrix remodeling and pro-fibrotic activity generally associated to an M2 function, was expressed at the highest levels in M2a macrophages cultured either on PCL films and scaffolds, with no significant difference among these conditions.

4. Discussion

Macrophages represent two faces of the inflammatory process, being involved in both beneficial and detrimental events, ranging from tissue healing and remodeling to the onset of chronic inflammation and inflammatory diseases [2,38]. Thus, therapeutic strategies targeting the modulation of macrophage behaviour and promoting the release of anti-inflammatory factors may open new opportunities for controlling inflammation [39]. Beyond the biochemical factors, macrophage phenotype can be regulated by biophysical cues provided by the 3D surrounding environment.

To create a defined microenvironment capable of providing appropriate cues, MEW has recently emerged as a promising approach that has a number of advantages. In contrast with scaffolds created from large filaments via fused deposition modelling (FDM) or microfiber scaffolds generated by the poorly controlled electrospinning process, MEW technology makes it possible generating micron-sized fibers on the same scale as cell bodies that are deposited according to a designed pattern. These highly defined scaffolds with controlled microfiber diameters and fiber orientations provide uniquely engineered cellular niches to better study and control cell response within 3D environments. This includes the impact of precisely placed microfibers on cell response within a 3D environment, such as providing guidance cues for nerve growth and glial cell migration [40] or the biomechanical influence of overlapping fibers angles, where these small scale geometries have been shown to drive the osteogenic differentiation of mesenchymal stromal cells [30]. More relevant to the current study is a recent report on the impact of precisely fabricated pore sizes and shape on macrophage cell phenotype [31]. While a general evaluation of macrophage phenotype was performed during this study, the findings clearly highlighted the ability of MEW to create defined pore geometries down to 40 μm in size and revealed how smaller pore sizes can drive a preferential phenotypic switch from an M0 to a generalized M2 macrophage state. In contrast, our study focuses on the ability of microfiber angle geometry to either sustain an existing macrophages phenotype (M0, M1, M2a, M2c) or promote the transition between various cell states, thereby mimicking different scenarios of scaffold implantation.

A consistent theme throughout the majority of MEW studies is the use of PCL, owing its low melting temperature (~60 °C) and resistance

to thermal degradation that lends itself to MEW processing. While other materials are starting to be explored, PCL is by far the most standardized and widely reported [41]. While the impact of material properties on macrophage polarization deserves further investigation for future MEW scaffold designs, the use of PCL in the current study better facilitates the comparison with existing literature. Furthermore, the status of PCL as a polymer with FDA approval for implantation opens the possibility of more easily translating these findings to the clinic [42,43].

Based on these premises, we evaluated the effect of the 3D architecture of PCL scaffolds on macrophage phenotype. Taking advantage of the MEW technique, we generated 3 different architectures with different pore geometries with well-defined inter-fiber angles to study their influence on macrophage behavior. Specifically, we investigated angles of 90°, 60°, 150° and 30°, which corresponded to different polygons as elementary unit of the scaffolds: square, triangle and rhombus. Using this technique, we managed to obtain fibers in the range of 17–20 μm, comparable to the cell dimension considering that the size of human macrophages is in the range of 11–20 μm [28,44,45]. Since cell elongation induced by the interaction of cells with scaffold fibers has been shown to drive M2 polarization of freshly-isolated monocytes [26,31] and murine macrophages [16], our aim was to investigate the influence of different scaffolds characterized by angles favoring or hampering the formation of cell bridges across fibers on the behavior of pre-differentiated unpolarized and polarized macrophages. The rationale for evaluating pre-polarized cell response is to emulate an implantation scenario where a scaffold would be introduced into a region that is potentially exhibiting different inflammatory conditions. Under this scenario, monocytes/macrophages could already be present in a polarized state in response to the signaling events resulting from the existing pathology, like in the case of inflammatory articular diseases or chronic tendinopathies, or from the implantation procedure. For what concerns polarized macrophages, we investigated the response to the scaffolds of M1, M2a and M2c phenotypes. The selected M2 phenotypes are known to contribute to the tissue healing process [46]. Other M2 phenotypes include the so-called M2b and M2d macrophages. M2b macrophages, beyond being associated with tumor progression, favor bacterial infections and play a key role in auto-immune and auto-inflammatory diseases [46], while M2d macrophages, also known as Tumor-Associated Macrophages (TAM), promote tumor development and tumor escape from the immune system [46,47]. Given the specific roles of M2b and M2d macrophages, they were not included in this study since we considered them as less biologically relevant in the context of an aseptic tissue healing process.

To distinguish the effect of different scaffold architectures on macrophage morphology, we cultured cells on both PCL 2D films and 3D scaffolds. We found that M0 as well as M2a and M2c macrophages cultured on PCL films showed a pancake morphology, while M1 macrophages displayed an elongated shape, as confirmed by the quantification of circularity and aspect ratio (Supplementary Figure SI5), and in line with previous studies [48,49]. It must be noted though that the relationship between cell morphology and human macrophage phenotype is still controversial, since some studies have described the pancake morphology as typical of M1 macrophages [50,51]. However, these studies used polarization protocols very different from the one used in our study, which may, at least partially, explain the different results obtained. The inconsistency among the existing literature data suggests that cell morphology alone can hardly be interpreted as a univocal index of macrophage polarization and needs to be supported by additional phenotypic and functional analyses. What emerged from our results was that, at least from a morphological point of view, when cultured on PCL films or scaffolds, M0 macrophages shared more similarities with M2a and M2c macrophages than with M1 macrophages. It was also observed that in correspondence of 90° and 60° angles, the cells formed "cell bridges", while in correspondence of the obtuse angle (150°) this did not occur. These results are partially in contrast with a previous study in which the elongation of monocyte-derived macrophages was detected in square-grid scaffold but not in the triangle-grid architecture [31]. This discrepancy is probably due to the smaller pore size of the triangle scaffold used in the above mentioned study that allowed cells to occupy almost the entire pore and not stretch across the pore, and indicated that cell response to pore geometry depends not only on pore shape and angle size, but also on pore dimension.

To evaluate the effect of the different scaffold architectures on macrophage polarization, we analyzed the expression of cell surface markers and the production of pro- and anti-inflammatory factors, in line with previous studies investigating the influence of scaffolds on macrophage polarization [26,31,52,53]. CD86, CD206, and CD163 were used to discriminate M1, M2a and M2c macrophages, being generally acknowledged as macrophage phenotypic markers [6,54]. The qualitative analysis of surface marker expression allowed detecting slight variations in the levels of these markers depending on the different macrophage phenotype. However, it should be underlined that, as confirmed by the flow cytometry data provided here, none of these markers is turned on or off based on macrophage polarization, rather any macrophage phenotype expresses all these markers but at different levels. Indeed, when the expression of these markers is analyzed by cytofluorimetry, variations in expression levels can be mainly visualized as shifts in the mean fluorescence intensity of cells rather than in changes in the percentage of positive cells, in line with the literature [55]. Hence, to analyze the polarization state, changes in more than one marker should be measured not only in terms of percentage of positive cells, but also in terms of expression levels, which resulted quite complicated through image analysis. Indeed, the use of immunofluorescence certainly represents a limitation of the current study, but it was initially intended to correlate surface marker expression with cell morphology. However, in our scaffolds cells mainly distributed along the fibers rather than across the pores, with the exception of cells forming bridges across angles, which most likely made difficult to appreciate changes in surface marker expression when analysing the same macrophage phenotype cultured on different scaffold architectures.

Given the intrinsic limitations of immunofluorescence, to evaluate the behaviour of macrophages in response to different scaffold architectures, we analyzed the secretory profile of pro- and anti-inflammatory proteins, as suggested by a previous study [56]. Despite we had initially selected typical M1 and M2 markers for this analysis, the macrophage response on TCP did not yield very clear differences among the different macrophage phenotypes. Although a high amount of pro-inflammatory cytokines was used to induce the macrophages towards a pro-inflammatory phenotype (i.e. 100 ng/mL IFNγ and 100 ng/mL TNFα), only few M1 markers were found to be upregulated in M1 macrophages compared to M0 macrophages on TCP. Indeed, the only markers that were robustly upregulated in M1 macrophages on TCP compared to the M0 condition were CXCL9 and CCL5. Similarly, CCL22 and sCD163 were the only markers consistently upregulated in M2a and M2c macrophages, respectively, on TCP compared to the M0 condition.

The lack of a strong upregulation of M1 markers may depend on the choice of a polarizing protocol based on IFNγ and TNFα [57,58], rather than the classical polarization protocol based on IFNγ and LPS [34]. The rationale of this choice lies in the idea of modelling an activation state related to an inflamed aseptic environment, resembling the implantation of biomaterials in an injured or inflamed tissue. Differently, the presence of LPS in the standard protocol simulates a bacterial infection. To confirm the effective polarization of macrophages towards an M1 phenotype, we have conducted supporting experiments that demonstrate that the polarization with IFNγ and TNFα induces a pattern of surface markers similar to that obtained with the classical polarization based on IFNγ and LPS (Supplementary Figure SI6). Another reason for the mild differences among phenotypes may be the removal of polarizing cytokines during macrophage culture on scaffolds, although we verified by flow cytometry that, after 3 days of culture without cytokines, unpolarized and polarized macrophages maintain distinct

phenotypes, with M1 macrophages being characterized by low levels of CD206 and CD163, that are instead highly expressed in M2a and M2c macrophages, respectively. Differently from similar studies that focus on the biomaterial-induced response of unpolarized macrophages [26,59,60], here the rationale for evaluating also the response of pre-polarized macrophages was to emulate an implantation scenario where a scaffold is introduced into a region that is potentially exhibiting different inflammatory conditions. Under this scenario, monocytes/macrophages could potentially be already polarized in response to the local signaling events resulting from either the existing condition that necessitates an implant or the implantation procedure itself. Pre-polarizing the macrophages was preferred to inducing their polarization during the culture on PCL scaffolds also to avoid that the high and supra-physiological concentrations of polarizing cytokines used to achieve macrophage polarization in vitro would completely overrule any possible effect of the scaffold geometry on cell phenotype, a very likely possibility based on our hands-on experience with primary human macrophages.

The analysis of the secretory profile of macrophages cultured on 3D scaffolds revealed that the rhombus architecture enhanced the secretion of both pro- and anti-inflammatory proteins from M0, M2a, and M2c macrophages. Of note, the simultaneous presence of acute and obtuse angles in the rhombus configuration represents a limitation that may complicate the interpretation of these outcomes, resulting in a dual effect on cell phenotype. However, it should be underlined that albeit the rhombus increased the secretion of IL1β, TNFα, and IL6 by M0 macrophages, the amount of these proteins was very low, if compared to the other markers analyzed. For instance, the release of IL1β in the rhombus scaffolds was balanced by the release of IL1Ra, the antagonist for IL1β receptor, which has a key role in the control of the inflammatory process [61]. Additionally, although the pro-inflammatory feature of IL1β and TNFα is undoubtable, IL6 has also anti-inflammatory properties [62], which means that an increase in its expression may not necessarily represent a negative event.

No clear differences were found between scaffold architectures for the release of anti-inflammatory proteins by M1 macrophages. In fact, M1 macrophages showed the lowest release of anti-inflammatory proteins compared to the other phenotypes independently from the scaffold architecture, suggesting that culture on 3D PCL scaffolds was not sufficient to induce the switch of M1 macrophages to M2 macrophages. Conversely, the rhombus enhanced the release of M2 typical markers, such as CCL17 and CCL24, by M0 and M2a macrophages compared to the other architectures and to the PCL film condition. Additionally, the rhombus architecture enhanced the secretion by M2a macrophages of IL10, IL13, IL18 and sCD163, with significant differences between the rhombus and the PCL film condition showing the ability of the 3D architecture over the material in promoting the secretion of these anti-inflammatory and pro-angiogenic markers. These, together with IL1Ra, were upregulated by the rhombus configuration also in M0 macrophages, although the difference with respect to M0 macrophages on PCL films was significant only for IL18.

Altogether our findings suggest that the rhombus architecture was more effective than the others in promoting the release of anti-inflammatory factors by M2a macrophage, but also by M0 macrophages. Being the same biomaterial used for the fabrication of all the scaffold architectures, the differences observed among the 3D architectures are directly dependent on the reaction of cells to scaffold geometry. The rhombus architecture, characterized by the presence of obtuse 150° angles, enhanced the presence of cells mainly along the fibers, as reported by a recent study where MEW was used to generate scaffolds with square and rhomboidal pores [30]. On the other hand, the square (90° angles) and the triangle (60° angles) architectures promoted the formation of "cell bridges" that were not visible in correspondence of obtuse angles. A recent study has demonstrated that mesenchymal stem cells have a tendency to branch across fibers in MEW-fabricated PCL scaffolds characterized by 90° and 45° angles, which resulted in greater cytoskeletal tension and nuclear localization of the transcriptional co-activator YAP. Differently, the localization of YAP is mainly cytoplasmic in cells aligned along the fibers of scaffolds characterized by obtuse angles [30]. This mechanism might also apply to human macrophages, where an increased nuclear localization of YAP has been correlated with a pro-inflammatory macrophage phenotype [63], but this hypothesis remains to be tested in our experimental set-up. Of note, the modulation of the YAP/TAZ signaling pathway is not the only mechanisms that could be potentially involved in the observed macrophage behavior. Indeed, there is a plethora of pathways that mediate macrophage response to topographical and mechanical cues [14,64]. For instance, the transcriptional regulator MRTF-A is a cytoplasmic actin-bound protein that, when freed upon actin polymerization, relocates to the nucleus where it activates inflammatory programs. The spatial confinement of macrophages has been shown to reduce the nuclear localization of MRTF-A by downregulating actin polymerization, thus resulting in a milder response to inflammatory signals [65]. Additionally, cell adhesion to scaffolds can lead to integrin clustering and subsequently activate, through a FAK-mediated process, multiple members of the Rho GTPases family that control actin cytoskeletal dynamics and are directly involved in the assembly of actin stress fibers, lamellipodia, and filipodia [14].

In our study, M0 macrophages cultured on the triangle and square scaffolds behaved almost similarly in terms of cytokine and chemokine secretion, in contrast with a previous study in which chitosan scaffolds with triangular pores have been shown to decrease the production of pro-inflammatory cytokines by freshly-isolated monocytes, when compared to square pores [26]. These differences may be due either to the cell source used, freshly-isolated monocytes vs. pre-differentiated macrophages, or to the different biomaterial chemistry and scaffold features. Indeed, beyond the different material used for scaffold fabrication, the scaffolds used in the study of Almeida et al. [26] were characterized by larger pore size (320–693 μm) and fiber diameter (220–280 μm), being far from cell dimension and from the fiber size (17–20 μm) of our scaffolds.

To summarize our findings, we observed that cells behave differently when in contact with different architectures, confirming the suitability of rational scaffold design, intended as the possibility to incorporate specific geometric features in scaffold architecture, to modulate macrophage behavior. These findings represent a starting point for our future research work in this field. Given the promising results provided by the rhombus architecture, we will try to optimize the fabrication settings to achieve scaffolds characterized only by obtuse angles, such as the honeycomb geometry, although fabricating this geometry is very complex due to the need of overlying two layers of fibers constituted by broken lines with sharp edges, which has so far resulted in a low accuracy of stacked layers. Additionally, given the recent work of Tylek et al. [31] who showed that, given a fixed pore geometry, pore size can be modulated to influence cell phenotype, we will take into consideration the fabrication of scaffolds with rhomboidal shape and smaller pore size to further exploit this scaffold geometry in the rational design of scaffolds able to positively influence macrophage behavior.

5. Conclusions

In this study, we have exploited MEW to evaluate how different scaffold architectures affect the expression and secretion of pro- and anti-inflammatory proteins by human macrophages. We demonstrated that the rhombus architecture increased the secretion of anti-inflammatory factors, especially if compared to culture on PCL films with no geometric cues, which may facilitate the generation of a tissue-healing environment. These findings therefore demonstrate that macrophages react to a specific 3D environment and represent a starting point for further investigation addressed to verify the molecular mechanisms responsible for macrophage response and the relevance of these findings in vivo.

Ethics approval and consent to participate

The primary human monocytes/macrophages used in this study are obtained from buffy coats purchased from a local blood bank. Buffy coats are provided in an anonymized form without providing donor gender, age, or any other relevant data. The buffy coat are used uniquely for monocyte isolation. The isolated cells are not used for any diagnostic and therapeutic purpose and no genetic investigation is conducted on cells. Based on all these considerations, ethics approval is not required for the isolation and use of these cells and blood donors are not required to provide any informed consent related to the use of the cells or to the publication of data derived from the use of these cells.

CRediT authorship contribution statement

Carlotta Mondadori: Conceptualization, Methodology, Investigation, Formal analysis, Data curation, Writing – original draft. **Amit Chandrakar:** Methodology, Investigation, Formal analysis, Resources. **Silvia Lopa:** Conceptualization, Methodology, Formal analysis, Data curation, Writing – original draft, revised manuscript, Visualization, Supervision. **Paul Wieringa:** Conceptualization, Methodology, Formal analysis, Data curation, Writing – original draft, revised manuscript, Supervision. **Giuseppe Talò:** Formal analysis, Visualization. **Silvia Perego:** Investigation, Formal analysis. **Giovanni Lombardi:** Formal analysis, Writing – review & editing, Funding acquisition. **Alessandra Colombini:** Investigation, Formal analysis. **Matteo Moretti:** Conceptualization, Methodology, Writing – review & editing, Supervision, Funding acquisition. **Lorenzo Moroni:** Conceptualization, Methodology, Writing – review & editing, Supervision, Funding acquisition.

Declaration of competing interest

Authors have no competing interest to declare.

Acknowledgements

We are grateful to Denis van Beurden for helping with SEM acquisition. This study was supported and funded by the Italian Ministry of Health (Ricerca Corrente), the Interreg NWE BONE Project (NWE497), and the project NeuroBeta with project number 15900 of the VENI research program which is financed by the Dutch Research Council (NWO). The data that support the findings of this study are available at the following link: https://osf.io/ju7x8/.

Appendix A. Supplementary data

Supplementary data to this article can be found online at https://doi.org/10.1016/j.bioactmat.2022.07.014.

References

[1] M.T. Silva, M. Correia-Neves, Neutrophils and macrophages: the main partners of phagocyte cell systems, Front. Immunol. 3 (2012) 174.
[2] Y. Oishi, I. Manabe, Macrophages in inflammation, repair and regeneration, Int. Immunol. 30 (11) (2018) 511–528.
[3] Y.R. Na, S. Je, S.H. Seok, Metabolic features of macrophages in inflammatory diseases and cancer, Cancer Lett. 413 (2018) 46–58.
[4] P.J. Murray, et al., Macrophage activation and polarization: nomenclature and experimental guidelines, Immunity 41 (1) (2014) 14–20.
[5] F.O. Martinez, et al., Macrophage activation and polarization, Front. Biosci. 13 (2008) 453–461.
[6] A. Mantovani, et al., The chemokine system in diverse forms of macrophage activation and polarization, Trends Immunol. 25 (12) (2004) 677–686.
[7] P.J. Murray, T.A. Wynn, Protective and pathogenic functions of macrophage subsets, Nat. Rev. Immunol. 11 (11) (2011) 723–737.
[8] N. Wang, H. Liang, K. Zen, Molecular mechanisms that influence the macrophage m1-m2 polarization balance, Front. Immunol. 5 (2014) 614.
[9] L. Parisi, et al., Macrophage polarization in chronic inflammatory diseases: killers or builders? J. Immunol. Res. 2018 (2018), 8917804.
[10] S.R. Hyam, et al., Arctigenin ameliorates inflammation in vitro and in vivo by inhibiting the PI3K/AKT pathway and polarizing M1 macrophages to M2-like macrophages, Eur. J. Pharmacol. 708 (1–3) (2013) 21–29.
[11] L. Utomo, et al., Guiding synovial inflammation by macrophage phenotype modulation: an in vitro study towards a therapy for osteoarthritis, Osteoarthritis Cartilage 24 (9) (2016) 1629–1638.
[12] R.D. Stout, et al., Macrophages sequentially change their functional phenotype in response to changes in microenvironmental influences, J. Immunol. 175 (1) (2005) 342–349.
[13] R.D. Stout, J. Suttles, Functional plasticity of macrophages: reversible adaptation to changing microenvironments, J. Leukoc. Biol. 76 (3) (2004) 509–513.
[14] F.Y. McWhorter, C.T. Davis, W.F. Liu, Physical and mechanical regulation of macrophage phenotype and function, Cell. Mol. Life Sci. 72 (7) (2015) 1303–1316.
[15] J.D. Bryers, C.M. Giachelli, B.D. Ratner, Engineering biomaterials to integrate and heal: the biocompatibility paradigm shifts, Biotechnol. Bioeng. 109 (8) (2012) 1898–1911.
[16] F.Y. McWhorter, et al., Modulation of macrophage phenotype by cell shape, Proc. Natl. Acad. Sci. U. S. A. 110 (43) (2013) 17253–17258.
[17] R. Sridharan, et al., Biomaterial based modulation of macrophage polarization: a review and suggested design principles, Mater. Today 18 (6) (2015) 313–325.
[18] B.M. Baker, C.S. Chen, Deconstructing the third dimension: how 3D culture microenvironments alter cellular cues, J. Cell Sci. 125 (Pt 13) (2012) 3015–3024.
[19] T.U. Luu, et al., Micro- and nanopatterned topographical cues for regulating macrophage cell shape and phenotype, ACS Appl. Mater. Interfaces 7 (51) (2015) 28665–28672.
[20] Y. Sun, et al., Electrospun fibers and their application in drug controlled release, biological dressings, tissue repair, and enzyme immobilization, RSC Adv. 9 (44) (2019) 25712–25729.
[21] E.M. Sussman, et al., Porous implants modulate healing and induce shifts in local macrophage polarization in the foreign body reaction, Ann. Biomed. Eng. 42 (7) (2014) 1508–1516.
[22] K. Garg, et al., Macrophage functional polarization (M1/M2) in response to varying fiber and pore dimensions of electrospun scaffolds, Biomaterials 34 (18) (2013) 4439–4451.
[23] Z. Wang, et al., The effect of thick fibers and large pores of electrospun poly (epsilon-caprolactone) vascular grafts on macrophage polarization and arterial regeneration, Biomaterials 35 (22) (2014) 5700–5710.
[24] E.D. Boland, et al., Electrospinning polydioxanone for biomedical applications, Acta Biomater. 1 (1) (2005) 115–123.
[25] E. Saino, et al., Effect of electrospun fiber diameter and alignment on macrophage activation and secretion of proinflammatory cytokines and chemokines, Biomacromolecules 12 (5) (2011) 1900–1911.
[26] C.R. Almeida, et al., Impact of 3-D printed PLA- and chitosan-based scaffolds on human monocyte/macrophage responses: unraveling the effect of 3-D structures on inflammation, Acta Biomater. 10 (2) (2014) 613–622.
[27] N.J. Hogrebe, J.W. Reinhardt, K.J. Gooch, Biomaterial microarchitecture: a potent regulator of individual cell behavior and multicellular organization, J. Biomed. Mater. Res. 105 (2) (2017) 640–661.
[28] T.D. Brown, P.D. Dalton, D.W. Hutmacher, Direct writing by way of melt electrospinning, Adv. Mater. 23 (47) (2011) 5651–5657.
[29] G. Hochleitner, et al., Additive manufacturing of scaffolds with sub-micron filaments via melt electrospinning writing, Biofabrication 7 (3) (2015), 035002.
[30] K.F. Eichholz, D.A. Hoey, Mediating human stem cell behaviour via defined fibrous architectures by melt electrospinning writing, Acta Biomater. 75 (2018) 140–151.
[31] T. Tylek, et al., Precisely defined fiber scaffolds with 40 mum porosity induce elongation driven M2-like polarization of human macrophages, Biofabrication 12 (2) (2020), 025007.
[32] T.M. Robinson, D.W. Hutmacher, P.D. Dalton, The next frontier in melt electrospinning: taming the jet, Adv. Funct. Mater. 29 (44) (2019), 1904664.
[33] S. Lopa, et al., Arthritic and non-arthritic synovial fluids modulate IL10 and IL1RA gene expression in differentially activated primary human monocytes, Osteoarthritis Cartilage 23 (11) (2015) 1853–1857.
[34] K.L. Spiller, et al., Differential gene expression in human, murine, and cell line-derived macrophages upon polarization, Exp. Cell Res. 347 (1) (2016) 1–13.
[35] N. Grotenhuis, et al., A culture model to analyze the acute biomaterial-dependent reaction of human primary macrophages, Biochem. Biophys. Res. Commun. 433 (1) (2013) 115–120.
[36] L. Utomo, et al., In vitro modulation of the behavior of adhering macrophages by medications is biomaterial-dependent, Biomed. Mater. 12 (2) (2017), 025006.
[37] L.P. Silva, et al., Measurement of DNA concentration as a normalization strategy for metabolomic data from adherent cell lines, Anal. Chem. 85 (20) (2013) 9536–9542.
[38] N. Fujiwara, K. Kobayashi, Macrophages in inflammation, Curr. Drug Targets - Inflamm. Allergy 4 (3) (2005) 281–286.
[39] A. Sica, A. Mantovani, Macrophage plasticity and polarization: in vivo veritas, J. Clin. Invest. 122 (3) (2012) 787–795.
[40] A. Hrynevich, et al., Design of suspended melt electrowritten fiber arrays for schwann cell migration and neurite outgrowth, Macromol. Biosci. 21 (7) (2021) e2000439.
[41] J.C. Kade, P.D. Dalton, Polymers for melt electrowriting, Adv. Healthc. Mater. 10 (1) (2021) e2001232.
[42] M.A. Abedalwafa, et al., Biodegradable poly-epsilon-caprolactone (PCL) for tissue engineering applications: a review, Rev. Adv. Mater. Sci. 34 (2013) 123–140.
[43] A. Cipitria, et al., Design, fabrication and characterization of PCL electrospun scaffolds—a review, J. Mater. Chem. 21 (26) (2011) 9419–9453.

[44] K. Menck, et al., Isolation of human monocytes by double gradient centrifugation and their differentiation to macrophages in teflon-coated cell culture bags, JoVE (91) (2014), e51554.
[45] F. Krombach, et al., Cell size of alveolar macrophages: an interspecies comparison, Environ. Health Perspect. 105 (Suppl 5) (1997) 1261–1263.
[46] L.X. Wang, et al., M2b macrophage polarization and its roles in diseases, J. Leukoc. Biol. 106 (2) (2019) 345–358.
[47] J. Zhou, et al., Tumor-associated macrophages: recent insights and therapies, Front. Oncol. 10 (2020) 188.
[48] E. Cassol, et al., M1 and M2a polarization of human monocyte-derived macrophages inhibits HIV-1 replication by distinct mechanisms, J. Immunol. 182 (10) (2009) 6237–6246.
[49] A. Toniolo, et al., Alternative activation of human macrophages is rescued by estrogen treatment in vitro and impaired by menopausal status, J. Clin. Endocrinol. Metab. 100 (1) (2015) E50–E58.
[50] F. Raggi, et al., Regulation of human macrophage M1-M2 polarization balance by hypoxia and the triggering receptor expressed on myeloid cells-1, Front. Immunol. 8 (2017) 1097.
[51] T. Buchacher, et al., M2 polarization of human macrophages favors survival of the intracellular pathogen Chlamydia pneumoniae, PLoS One 10 (11) (2015) e0143593.
[52] V. Ballotta, et al., Strain-dependent modulation of macrophage polarization within scaffolds, Biomaterials 35 (18) (2014) 4919–4928.
[53] T.B. Wissing, et al., Hemodynamic loads distinctively impact the secretory profile of biomaterial-activated macrophages - implications for in situ vascular tissue engineering, Biomater. Sci. 8 (1) (2019) 132–147.
[54] F.R. Bertani, et al., Classification of M1/M2-polarized human macrophages by label-free hyperspectral reflectance confocal microscopy and multivariate analysis, Sci. Rep. 7 (1) (2017) 8965.
[55] K.L. Spiller, et al., The role of macrophage phenotype in vascularization of tissue engineering scaffolds, Biomaterials 35 (15) (2014) 4477–4488.
[56] M. Bartneck, et al., Inducing healing-like human primary macrophage phenotypes by 3D hydrogel coated nanofibres, Biomaterials 33 (16) (2012) 4136–4146.
[57] E. Ragni, et al., Inflammatory priming enhances mesenchymal stromal cell secretome potential as a clinical product for regenerative medicine approaches through secreted factors and EV-miRNAs: the example of joint disease, Stem Cell Res. Ther. 11 (1) (2020) 165.
[58] L. Utomo, et al., Cartilage inflammation and degeneration is enhanced by pro-inflammatory (M1) macrophages in vitro, but not inhibited directly by anti-inflammatory (M2) macrophages, Osteoarthritis Cartilage 24 (12) (2016) 2162–2170.
[59] S.E. Blatt, et al., Characterizing the macrophage response to immunomodulatory biomaterials through gene set analyses, Tissue Eng. C Methods 26 (3) (2020) 156–169.
[60] C.E. Witherel, et al., Response of human macrophages to wound matrices in vitro, Wound Repair Regen. 24 (3) (2016) 514–524.
[61] C.A. Dinarello, Overview of the IL-1 family in innate inflammation and acquired immunity, Immunol. Rev. 281 (1) (2018) 8–27.
[62] J. Scheller, et al., The pro- and anti-inflammatory properties of the cytokine interleukin-6, Biochim. Biophys. Acta 1813 (5) (2011) 878–888.
[63] V.S. Meli, et al., YAP-mediated mechanotransduction tunes the macrophage inflammatory response, Sci. Adv. 6 (49) (2020).
[64] V.S. Meli, et al., Biophysical regulation of macrophages in health and disease, J. Leukoc. Biol. 106 (2) (2019) 283–299.
[65] N. Jain, V. Vogel, Spatial confinement downsizes the inflammatory response of macrophages, Nat. Mater. 17 (12) (2018) 1134–1144.